

*Revised and returned*

# Revised phase diagram for the Pt-Ti system from 30 to 60 at.% platinum

T. Biggs<sup>a,b</sup>, L.A. Cornish<sup>a,c</sup>, M.J. Witcomb<sup>d</sup> and M.B. Cortie<sup>a,e</sup>

<sup>a</sup>Physical Metallurgy Division, Mintek, Private Bag X3015, Randburg 2125, South Africa

<sup>b</sup>now at 44 Kildonan Cr, Waterdown, ON, L0R 2H5, CANADA

<sup>c</sup>School of Process and Materials Engineering, University of the Witwatersrand, Priv. Bag 3, WITS 2050, South Africa

<sup>d</sup>Electron Microscope Unit, University of the Witwatersrand, Private Bag 3, WITS 2050, South Africa

<sup>e</sup>Institute for Nanoscale Technology, University of Technology Sydney, PO Box 123, Broadway, NSW 2007, Australia

---

## Abstract

Alloys of the Ti-Pt system between 30 and 61 at.% Pt were studied using metallography with optical and scanning electron microscopy, X-ray diffraction, and differential thermal analysis. A phase of nominal composition  $\text{Ti}_4\text{Pt}_3$ , in the range 41.7 - 43.4 at.% Pt was found in samples containing between 30 and 47 at.% Pt, and was apparently formed by a peritectoid reaction between  $\beta\text{-TiPt}$  and  $\text{Ti}_3\text{Pt}$  at  $1205 \pm 10^\circ\text{C}$ . The eutectic reaction between  $\text{Ti}_3\text{Pt}$  and  $\beta\text{-TiPt}$  was found to be at  $\sim 35$  at.% Pt and  $1424 \pm 10^\circ\text{C}$ , and the  $\text{Ti}_3\text{Pt}$  phase melted at circa  $1500^\circ\text{C}$ . The other phase boundaries agreed with published literature, except that a slightly wider range was found at  $1200^\circ\text{C}$  for  $\beta\text{-TiPt}$ .

**Keywords :** A. metals, B. casting, E. thermal analysis

---

## 1. Introduction

The TiPt phase is of interest because it undergoes a reversible B2  $\leftrightarrow$  B19 martensite transformation at  $\sim 1000^\circ\text{C}$  [1,2] which could give it the potential for the shape memory effect (SME) at this temperature. However, uncertainty in the published phase diagram has been expressed [2-4], particularly in respect of relationships between about 25 at.% Pt and 45 at.% Pt. In addition, the steep liquidus on the Ti-rich side of the TiPt phase ensures that samples of sub-stoichiometric TiPt are likely to contain Ti-rich phases due to coring during solidification, which may impact on the possible use of this material as a shape memory alloy. Therefore, it is of importance to establish the true nature of the phase diagram on the Ti-rich side of TiPt.

## 2. Previous Work

Nishimura and Hiramatsu [5] undertook the most comprehensive study of the Pt-Ti phase diagram, using metallography, X-ray analysis and differential thermal analysis, although four other phases have been found subsequently [4]. Nishimura and Hiramatsu found three intermetallic phases:  $\text{Ti}_3\text{Pt}$ , TiPt and  $\text{TiPt}_3$ , which they reported as melting congruently at the respective temperatures of  $1370^\circ\text{C}$ ,  $1830^\circ\text{C}$  and  $1950^\circ\text{C}$ . They also reported three eutectic reactions: the first forming  $\beta$ -Ti and  $\text{Ti}_3\text{Pt}$  at  $\sim 15$  at.% Pt and  $1310^\circ\text{C}$ ; the second forming  $\text{Ti}_3\text{Pt}$  and TiPt at  $\sim 34$  at.% Pt and  $1320^\circ\text{C}$ , and the third producing TiPt and  $\text{TiPt}_3$  at  $\sim 58$  at.% Pt and  $1780^\circ\text{C}$ . Sinha [6] reported that the phases in the latter eutectic were most likely  $\beta$ -TiPt and  $\text{Ti}_3\text{Pt}_5$ , and that at lower temperatures, the  $\text{Ti}_3\text{Pt}_5$  phase decomposed eutectoidally to form  $\alpha$ -TiPt and  $\text{TiPt}_3$ . Further work by Murray [3,4] and Meschter and Worrell [7] on these platinum-rich phases resulted in the phase diagram of Murray, which is redrawn here as Figure 1.

The crystal structures for the  $\alpha$ -TiPt and  $\text{Ti}_3\text{Pt}$  phases were derived by Dwight *et al.* [8] to be *oP4* (AuCd prototype) for  $\alpha$ -TiPt, and *cP8* ( $\text{Cr}_3\text{Si}$  prototype) for  $\text{Ti}_3\text{Pt}$ . Lattice parameters of  $\text{Ti}_3\text{Pt}$  were reported by Duwez and Jorden [9], Nishimura and Hiramatsu [5], Pietrokowsky [10], van Reuth and Waterstraat [11] and Junod *et al.* [12] and were found to be in good agreement at  $\sim 0.503$  nm for 25 at.% Pt. Additionally, Junod *et al.* [12] reported that the lattice parameter increased with increasing Pt content over the range 23-27 at.% Pt. Nishimura and Hiramatsu [5] did not determine the structure of the TiPt they found, and only Donkersloot and van Vucht [1] reported the high temperature  $\beta$ -TiPt. On the other hand, the low temperature form was identified and studied by Dwight *et al.* [8], Schubert *et al.* [13] and Raman and Schubert [14], and Donkersloot and van Vucht [1]. Krautwasser *et al.* [15] studied the structure of  $\text{Ti}_3\text{Pt}_5$  and found it to be *oI32* ( $\text{Au}_5\text{GaZn}_2$  prototype).

Donkersloot and van Vucht [1] found that the Pt-rich boundary of TiPt was  $\sim 54$  at% above  $600^\circ\text{C}$  because a 55 at.% Pt alloy demonstrated precipitation of  $\text{TiPt}_3$ , whereas a 52.5 at.% Pt alloy remained single phase. They also noted that a splat-cast sample of 45 at.% Pt precipitated  $\text{Ti}_3\text{Pt}$  on heating to  $600^\circ\text{C}$ , which indicates the position of the  $\alpha$ -TiPt solvus. They observed the B2  $\leftrightarrow$  B19 phase transformations of the TiPt phase using high temperature X-ray diffraction and DTA, but reported that the  $M_s$  (martensite start) temperatures were higher than the  $A_s$  (austenite start) temperatures, which is not possible for a simple, two-phase martensitic transformation cycle. They found that the  $M_s$  tended to increase with increasing Pt content, except that there was a sudden drop of  $\sim 50^\circ\text{C}$  between 50 and 52 at.% Pt. Biggs *et al.* [2] showed that the true  $M_s$  temperatures were approximately  $40^\circ\text{C}$  lower than those reported by Donkersloot and van Vucht [1]. This was because they found intermediate transformations for alloys below 50 at.% Pt, and concluded that there were at least two intermediate phases on cooling, and at least one on heating.

The compilation after Murray [4] (Figure 1) was utilized as a basis for a study of the TiPt

transformation [2], and for the present investigation of the phase relationships between  $\text{Ti}_3\text{Pt}$  and  $\beta\text{-TiPt}$ .

A problem in the study of this phase diagram is that titanium has a very high affinity for oxygen, and there may be some phases present which are actually oxides rather than pure binary intermetallic compounds. The work of at least Meschter and Worrell [7] and Jacob and Alcock [16] was affected by the presence of oxygen in the samples, and their activity data can therefore only be used as an approximation of the binary Ti-Pt system. At one stage, Murray [3] doubted that  $\text{Ti}_3\text{Pt}$  was a binary phase on the basis of Krautwasser's observation [15] that it was stabilized by oxygen, and was therefore a ternary phase. However, using purer alloys, van Reuth and Waterstraat [11] verified its integrity as a binary phase. Nevitt *et al.* [17] reported a  $\text{Ti}_2\text{Pt}$  phase which only formed in the presence of oxygen, and had the composition: 57.3 Ti - 28.6 Pt - 14 O (at.%).

### 3. Experimental Procedure

The alloy samples (~2 g each) were made from pure elements (99.2% purity for Ti and 99.8% purity for Pt) by arc-melting in a tungsten arc furnace with a copper cooled hearth, under spectrographic-grade argon and using a Ti getter for oxygen. Samples were examined in the as-cast condition, and also after a variety of heat treatments at, for example, 500°C, 800°C, 1000°C and 1200°C under vacuum, or under a gentle flux of spectrographic-grade argon. However, even spectrographic-grade argon contains of the order of a part per million trace impurity of oxygen and water, both of which will have readily reacted with the titanium of the samples, and which would have been continuously replenished under flowing conditions.

The samples were either furnace cooled, or water quenched. Analyses were conducted at two different laboratories using JEOL-840 scanning electron microscopes operating at 20kV and equipped with LINK AN10000 and Tracor software respectively. Additionally, an ARL SEMQ microprobe with Advanced Microbeam Inc. software at 15kV was also used on some samples. The results from the different machines from five samples in the range ~31 - 63 at.% Pt were compared against each other, and against the microprobe, as well as with chemical analysis undertaken by inductively coupled plasma optical - emission spectroscopy (ICP-OES) and the results agreed to within 1 at.%. X-ray diffraction was undertaken using a Siemens D500 diffractometer with  $\text{Mo K}_\alpha$  radiation. Peaks were compared with JCPDS data [18] as well as those calculated from the Crystallographica [19] program. Differential thermal analysis was carried out at two independent laboratories, both using Setaram TG-DTA 92 instruments.

### 4. Results

The EDS analyses of all the alloys are given in Table 1, and the phases were identified from these analyses, as well as comparison of the XRD spectra with available data. In addition, three alloys of 49.5, 50.2 and 53.8 at.% Pt were single phase  $\alpha\text{-TiPt}$  in the as-cast condition and are not described further here.

The as-cast alloys in the composition range 30-43 at.% Pt contained a phase of a previously unreported composition: 41.7 - 43.4 at.% Pt, which will be denoted as  $\text{Ti}_4\text{Pt}_3$ . In the 30.4 at.% Pt sample, this phase was present at the grain boundaries of  $\text{Ti}_3\text{Pt}$ , sometimes in a eutectic-like form, sometimes appearing as a continuous phase. Alloys between 36.3 and 40.9 at.% Pt showed dendrite-shaped regions of  $\text{Ti}_4\text{Pt}_3$  surrounded by a eutectic, sometimes sparse, of  $\text{Ti}_4\text{Pt}_3 + \text{Ti}_3\text{Pt}$  (Figure 2). As the Pt content increased, the relative proportion of the dendrite-like regions increased.

As-cast alloys of 42.7 and 43.1 at.% Pt had dendrite-like regions of  $\text{Ti}_4\text{Pt}_3$  surrounded by the  $\text{Ti}_4\text{Pt}_3 + \text{Ti}_3\text{Pt}$  eutectic, with a central core of  $\alpha\text{-TiPt}$  which was in the form of irregular laths (Figure 3). The  $\text{Ti}_3\text{Pt}$  phase within the eutectic had a different morphology from those samples with less platinum, and it is suspected that this had oxidized during sample preparation to become a ternary phase containing oxygen. Heat treating at  $800^\circ\text{C}$  increased the proportion of  $\text{Ti}_4\text{Pt}_3$  (Figure 4). As the Pt content was increased, the lath-like appearance of  $\text{TiPt}$  was observed in a higher proportion within the dendrite-like  $\text{Ti}_4\text{Pt}_3$ . At  $\sim 47$  at.% Pt, which is in excess of the equilibrium  $\text{TiPt}$  phase boundary, the bulk of the sample was  $\alpha\text{-TiPt}$ , but there was still a rim of  $\text{Ti}_4\text{Pt}_3$  coating the  $\text{TiPt}$  dendrites and an intergranular eutectic (Figure 5).

The XRD peaks of samples comprised predominantly of  $\text{Ti}_3\text{Pt}$ ,  $\alpha\text{-TiPt}$  and  $\text{Ti}_3\text{Pt}_5$  agreed well with those from the JCPDS database [18]. However, samples containing  $\text{Ti}_4\text{Pt}_3$  phase had additional peaks, in particular those corresponding to  $d \approx 2.64$  and  $1.95 \text{ \AA}$ . The peaks ostensibly generated by the  $\text{Ti}_4\text{Pt}_3$  phase are given in Table 2, and the list was derived by comparing the spectra of samples containing  $\text{Ti}_4\text{Pt}_3$  with the those of known  $\text{Ti}_3\text{Pt}$  and  $\text{TiPt}$  samples, and eliminating the common peaks. The XRD spectrum of a sample that was predominantly comprised of  $\text{Ti}_4\text{Pt}_3$  is compared in Figure 6 to the standard data for  $\text{Ti}_3\text{Pt}$  and  $\alpha\text{-TiPt}$ . The structure of  $\text{Ti}_4\text{Pt}_3$  could not be matched within the JCPDS database, and so is considered unique.

The samples near 50 at.% Pt were single phase, or near-single phase  $\alpha\text{-TiPt}$  which had transformed on cooling to give the characteristic plates from a martensite-like reaction. A sample with 55.6 at.% Pt (Figure 7) comprised dendrites of  $\alpha\text{-TiPt}$  surrounded by an eutectic of  $\text{TiPt}$  and a phase of low average atomic number (dark color) and substantial content of light elements (deduced from the low totals in the EDS analysis). The  $\text{TiPt}$  could be readily identified by its lath-like morphology. In order to derive more information regarding this phase, the LINK software was utilized to derive the volume fraction of it, assuming it to contain oxygen. This value (13 %) was then used to estimate the formula of the dark phase, which came to be  $\text{Ti}_2\text{Pt}(\text{O})$ . The presence of this phase, rather than  $\text{Ti}_3\text{Pt}_5$  or  $\text{TiPt}_3$ , is evidence that this particular sample was oxidized. The samples with 55.3 and 61.3 at.% Pt contained  $\alpha\text{-TiPt}$  and  $\text{Ti}_3\text{Pt}_5$  in a eutectic microstructure, as expected from the published phase diagram, together with a small amount of an oxygen-rich phase.

The oxidation problem has been previously encountered by other workers [7,16] was especially problematic in the present heat-treated alloys. Nevitt *et al.* [17] reported a ternary  $\text{Ti}_2\text{Pt-O}$  phase, whereas Donkersloot and van Vucht [1] reported  $\text{TiO}$  to precipitate in alloys of between  $\sim 40\text{-}50$  at.% Pt. Although the present heat treated samples all oxidized to some extent were therefore of limited use to the binary Ti-Pt investigation, they could still be used to confirm some of the deductions from the as-cast alloys. For example, samples containing between 40.7 and 43.1 at.% Pt were heat treated at  $1200^\circ\text{C}$  and furnace cooled, and were found to contain  $\alpha\text{-TiPt}$  in coarser form,  $\text{Ti}_4\text{Pt}_3$ , and large irregular particles of  $\text{Ti}_3\text{Pt}(\text{O})$ . However, a sample with  $\sim 43.4$  at.% Pt did not have any  $\text{Ti}_4\text{Pt}_3$ , and instead was mostly  $\alpha\text{-TiPt}$  with islands of the  $\text{Ti}_3\text{Pt}(\text{O})$  and  $\text{Ti}_2\text{Pt}(\text{O})$  phases. However, heat treatment of a 42.4 at.% Pt at  $800^\circ\text{C}$ , although only for an hour, appeared to reduce the amount of the  $\alpha\text{-TiPt}$ .

The oxides were recognized firstly by the lower EDS totals and secondly by their slightly different morphology. The EDS measurements of the oxides had totals of  $\sim 92\%$ , whereas the un-oxidized phases had totals very nearly equal to 100%. The EDS analyses of the oxide phases indicated Pt contents in the range 30-38 at.% Pt, with a cluster around  $\sim 34$  at.% Pt. The 34 at.% Pt phase,  $\text{Ti}_2\text{Pt}(\text{O})$ , was assumed to be an exclusively ternary phase, since  $\text{Ti}_2\text{Pt}$  has not been found in the Pt-Ti binary. If the ternary oxide phase is assumed to have an approximate composition 53 Ti: 29 Pt: 14 O (at.%), then ignoring oxygen (which was not detectable by the current EDS apparatus), values

of 33-34 at.% Pt could have been obtained. If the oxygen content was different in different alloys, then different values of Pt would have been obtained because the alloys would be on different tie-lines.

Differential thermal analysis was undertaken on most of the samples, starting with material in the as-cast state, and each run was undertaken up to three times, until it was realized that the results varied systematically on each subsequent run, probably due to oxidation of the samples. For example, the liquidus peak for the first heating run of the 30.4 at.% Pt sample occurred over the range 1448-1500°C, whereas the range for the second heating run was 1402-1443°C (with a similar decrease for the cooling runs). Thereafter, only results from the first run were used. These showed a definite pattern, whereas if the results of all three runs were plotted, there was much scatter [20]. Phase transformations were commonly observed at approximately 1030°C, 1215°C and 1440°C (Figure 8). The  $\sim 1030^\circ\text{C}$   $\alpha\text{-TiPt} \leftrightarrow \beta\text{-TiPt}$  transformation has been discussed elsewhere [2], and will not be discussed further here. The transformations at  $\sim 1205^\circ\text{C}$  and  $\sim 1425^\circ\text{C}$  were observed in the 30 - 45 at.% Pt range. Samples of 43 at.% and 45 at.% Pt only showed very small peaks at  $\sim 1430^\circ\text{C}$ . However, after some oxidation of the material had occurred, the 30 - 32 at.% Pt samples developed broad peaks between 1370°C and 1400°C. From inspection of the specimens, these were deduced to have been associated with melting.

The cooling curves (Figure 9) showed the expected undercooling, to the extent that the ‘slushy’ zone between liquidus and solidus has been suppressed in samples containing between 31 and 37% Pt, and replaced with a strong solidification peak (designated ‘A’ on Figure 9), presumably directly into the eutectic composition. The liquidus of the samples with 40, 43 and 44% Pt lay beyond the range of the scan so they did not show a solidification peak on cooling. The peritectoid reaction (‘B’) and the  $\beta \rightarrow \alpha$  reaction in TiPt is also clearly visible on the cooling curves. There are, however, some unexplained small peaks too, just possible due to solidification of the oxygen-containing phases previously discussed.

## 5. Discussion

The phase boundaries of  $\text{Ti}_3\text{Pt}$ , TiPt and  $\text{Ti}_3\text{Pt}_5$  show good agreement with those reported by previous workers, and the XRD peaks of these phases matched those on the JCPDS database. The higher Pt content reported for the  $\text{Ti}_3\text{Pt}$  in the 41.6 at.% Pt alloy is likely to have been an effect of the higher Pt content of the phases surrounding the fine  $\text{Ti}_3\text{Pt}$ , although two other alloys showed that the Pt-rich boundary of  $\text{Ti}_3\text{Pt}$  could be higher ( $\sim 31\text{-}32$  at.% Pt) than the reported 30 at.% [4]. However, the typical error of the present EDS was  $\sim 1$  at.%. Results of the  $\alpha\text{-TiPt}$  phase from heat treated samples appear anomalous in apparently having nearly a stoichiometric composition, but these results may be interpreted as showing that there is very little extension of that phase into the ternary Ti-Pt-O system. One alloy suggested that the Pt-rich boundary was higher than previously reported at  $1200^\circ\text{C}$ ,  $\sim 55$  rather than 53 at.% Pt.

The finding of a  $\alpha\text{-TiPt} \rightarrow \beta\text{-TiPt}$  transformation at  $\sim 1030^\circ\text{C}$  was in agreement with data from Donkersloot and van Vucht [1], and in fact clarified the reaction because the apparent anomaly of an  $M_s$  lying above the  $A_s$  was explained as being due to the presence of at least two intermediate phases [2].

The as-cast microstructures, chemical analyses and X-ray diffraction results are consistent with the presence of a new phase of nominal  $\text{Ti}_4\text{Pt}_3$  stoichiometry, and its formation by either a peritectic or peritectoid reaction, since the remnants of the parent phase are within the dendrites. Thus, either direct solidification to TiPt occurred subsequent to a peritectic reaction, or the peritectoid reaction did not run to completion. Therefore, alloys below the eutectic point would have  $\text{Ti}_3\text{Pt}$  as the

primary phase, and those between ~35 and 43 at.% Pt would have been primary TiPt, which reacted peritectoidally to form  $\text{Ti}_4\text{Pt}_3$ . Since there would have been less TiPt formed in this range (from the lever rule), the TiPt would be consumed in the reaction, leaving none. The presence of a reaction at ~1205°C, and the nature of the microstructures strongly suggests that  $\text{Ti}_4\text{Pt}_3$  is formed by a peritectoid rather than a peritectic reaction. Alloys above ~45 at.% Pt and below 50 at.% Pt would have more primary  $\beta$ -TiPt which would not be fully consumed in the peritectoid reaction. In as-cast samples, especially arc-melted samples, the reaction would be extremely unlikely to run to completion anyway due to the rapid rate of cooling, and residual primary phase would result. Of course, in this system there is the further complication of the  $\beta$ -TiPt  $\rightarrow$   $\alpha$ -TiPt transformation at ~1030°C which probably accounts for the lath-like structure. The explanation of Donkersloot and van Vucht's reported  $\text{Ti}_3\text{Pt}$  precipitation in a splat-cast 45 at.% Pt alloy [1], instead of  $\text{Ti}_4\text{Pt}_3$  could be due to their not using EDS or WDS to analyze the precipitates, or perhaps to the solidification during splat casting being sufficiently fast to suppress the peritectoid reaction at ~1214°C. The microstructure of their 45 at.% Pt alloy [1] agrees with the observation here that there was no  $\text{Ti}_4\text{Pt}_3$  observed in the 44.6 at.% Pt alloy, or that there was too little present to give a signal. The peritectoid reaction would also explain the irregular boundaries of the particles in the eutectic structures; this is because  $\text{Ti}_4\text{Pt}_3$  formed at the  $\text{Ti}_3\text{Pt}$ /TiPt boundaries, then the interfaces moved outwards slightly changing the morphologies of the original structures.

The evidence for the peritectoid nature of formation is also shown by the DTA results. There were peaks at ~1205°C and ~1424°C for a series of alloys: 31, 35, 38, 41, 44, and 45 at. % Pt which had undergone DTA up to 1520°C, although the higher temperature peaks were very small for the two alloys of higher Pt content. This can only be interpreted as a peritectoid reaction at ~1205°C and a eutectic reaction at ~1424°C. If the reaction was peritectic, no peak would exist at ~1424°C below 43 at.% Pt, except for one point on the  $\text{Ti}_3\text{Pt}$  liquidus. The reactions at higher temperatures (> 1445°C) would then be the liquidus. This agrees with the observation that the four alloys of lower Pt content melted, whereas the alloys of 43 and 45 at.% Pt did not. The slope of the liquidus above the  $\text{Ti}_3\text{Pt}$  phase was comparatively shallow. The 32.2 at.% Pt sample showed a peak at 1372°C, which was not explained. The DTA analyses indicate a very steep liquidus above the TiPt phase, which is also found on the assessed phase diagram [3,4]. A plot of the enthalpies of transformation of the presumed reverse peritectoid transformation is also interesting (Figure 10). It is evident that the enthalpy per gram of sample is a maximum at about the  $\text{Ti}_4\text{Pt}_3$  stoichiometry, as expected from a consideration of the volume fraction that the new phase would occupy in the microstructure. The failure of Nishimura and Hiramatsu [5] to find the  $\text{Ti}_4\text{Pt}_3$  phase can possibly be attributed to their sparse sampling of the region between 25 and 50 at% Pt, and a lack of access at that time to EDS and back-scattered scanning electron imagery.

The revised TiPt phase diagram is shown here as Figure 11. Also plotted on the diagram is the revised position of the  $\beta$ -TiPt to  $\alpha$ -TiPt displacive transformation, taken from the data of Biggs *et al.* [2].

The other major disagreement between the present work and that of Nishimura and Hiramatsu is the higher melting temperature of  $\text{Ti}_3\text{Pt}$ . They only drew one data point near  $\text{Ti}_3\text{Pt}$  and for 25 at.% Pt. As the number of DTA cycles increased in this work, the melting temperature of  $\text{Ti}_3\text{Pt}$  decreased, for example, the 30.4 at.% Pt alloy had the highest peak (associated with melting) occurring at 1448-1514°C on the first run, and 1402-1443°C on the second run. This appears to be due to oxidation of the  $\text{Ti}_3\text{Pt}$  phase to form  $\text{Ti}_3\text{Pt}(\text{O})$  with an associated decrease in melting temperature. It seems possible that the samples of Nishimura and Hiramatsu had oxidized, and their value represents the stable value of  $\text{Ti}_3\text{Pt}(\text{O})$ . The same is likely to be true for their lower eutectic temperature (1370°C compared with the present ~1427°C). This investigation has already indicated that the  $\text{Ti}_4\text{Pt}_3$  phase does not penetrate very far into the Pt-O-Ti ternary, and that there are reactions

between both  $\text{Ti}_3\text{Pt}(\text{O})$  and  $\text{Ti}_2\text{Pt}(\text{O})$  oxides (the latter at least eutectic in nature) and  $\beta\text{-TiPt}$ , as well as between  $\text{Ti}_4\text{Pt}_3$  and the  $\text{Ti}_3\text{Pt}(\text{O})$  oxide. Thus, it seems likely that if Nishimura and Hiramatsu's samples were contaminated with oxygen, they would be measuring the oxygen-containing eutectic within the ternary system, rather than the binary eutectic. Their  $\sim 1300^\circ\text{C}$  eutectic temperature agrees with temperatures recorded in this investigation for samples between 36.3-38.3 at.% Pt on the second and third DTA cycle.

Realizing that the oxygen-containing phase is present in some of the as-cast samples, and all of the heat treated samples, means that some features of the ternary phase diagram can be deduced. Firstly, since the  $\alpha\text{-TiPt}$  and  $\text{Ti}_4\text{Pt}_3$  phases did not have oxygen (they always had  $\sim 100\%$  totals for the EDS analyses, and with the microprobe), information gleaned for the binary Pt-Ti phase diagram is not thought to be compromised. Furthermore, these two phases are evidently confined to the binary edge of the ternary phase diagram. However, they take part in ternary reactions with a oxygen-containing phase.

## 6. Conclusions

A previously unreported phase of  $\text{Ti}_4\text{Pt}_3$  was found in alloys of 30.4 - 45.3 at.% Pt. The width of the field was 41.7 - 43.4 at.% Pt and the formation was by a peritectoid reaction of  $\beta\text{-TiPt}$  and  $\text{Ti}_3\text{Pt}$  at  $1205 \pm 10^\circ\text{C}$ . The eutectic reaction between  $\text{Ti}_3\text{Pt}$  and  $\text{TiPt}$  was at  $\sim 35$  at.% Pt and  $\sim 1424 \pm 10^\circ\text{C}$ , not the reported  $1320^\circ\text{C}$ , which was concluded to be the reaction from oxygen-contaminated samples. Additionally,  $\text{Ti}_3\text{Pt}$  was found to melt at  $\sim 1500^\circ\text{C}$ , not  $1370^\circ\text{C}$  as previously reported. The other phase boundaries were in good agreement with the literature, although  $\beta\text{-TiPt}$  had a slightly wider range at  $1200^\circ\text{C}$ .

## Acknowledgements

The authors thank Dr. J. Hohls, P. Ellis and V. Viljoen for assistance with DTA, SEM and WDS respectively. MJW thanks the University of the Witwatersrand for financial support via the Microstructural Studies Research Programme.

## 7. References

1. H.C. Donkersloot and J.H.N. van Vucht, *J. Less-Common Metals*, 20 (1970) 83-91.
2. T. Biggs, M.B. Cortie, M.J. Witcomb and L.A. Cornish, *Metall. and Mater. Trans. A*, 32A (2001) 1881-1886.
3. J.L. Murray, *Bull. Alloy Phase Diagrams*, 3 (1982) 329-334.
4. J.L. Murray, in *Binary Phase Diagrams*, Ed. T.B. Massalski, ASM, Ohio, 1986, pp. 1915-1917.
5. H. Nishimura and T. Hiramatsu, *Nippon Kinzoku Gakkaishi*, 21 (1957) 469-473.
6. A.K. Sinha, *Trans. AIME*, 245 (1969) 237-240.
7. P.J. Meschter and W.L. Worrell, *Metall. Trans. A*, 7 (1976) 299-305.
8. A.E. Dwight, R.A. Conner and J.W. Downey, *Acta Cryst.* 18 (1965) 835-839.
9. P. Duwez and C.B. Jorden, *Acta Cryst.* 5 (1952) 213-214.
10. P. Pietrokowsky, *Nature* 206 (1965) 291.
11. R.C. van Reuth and R.M. Waterstraat, *Acta Crystallogr.*, B24 (1968) 186-196.
12. A. Junod, R. Flukiger and J. Muller, *J. Phys. Chem. Solids*, 37 (1976) 27-31.
13. K. Schubert, A. Raman and W. Rossteutscher, *Naturwissenschaften*, 51 (1964) 505-507.
14. A. Raman and K. Schubert, *Z. Metallkd.*, 55 (1964) 704-710.
15. P. Krautwasser, S. Bhan and K. Schubert, *Z. Metallkd.*, 59 (1968) 724-729.
16. T. Jacob and C.B. Alcock, unpublished data cited by [76Mes].
17. M.V. Nevitt, J.W. Downey and R.A. Morris, *Trans AIME*, 218 (1960) 1019-1023.

*Revised and returned*

18. JCPDS (Joint Committee on Powder Diffraction Samples), PDF 2, Sets 1-45, International Centre for Diffraction Data, Pennsylvania, USA, 1995.
19. Crystallographica, Oxford Cryosystems, Version 1.31, 1997, [www.oxfordcryosystems.co.uk](http://www.oxfordcryosystems.co.uk).
20. T. Biggs, An Investigation into Displacive Transformations in Platinum Alloys, Ph.D. Thesis, University of the Witwatersrand, 2001.



Figure 1. Ti-Pt phase diagram after Murray [1].

Figure 2. SEM image in backscattered mode of 37.6 at.% Pt, arc-melted, showing peritectoid conversion and growth of prior TiPt dendrites to  $\text{Ti}_4\text{Pt}_3$  (grey), with sparse eutectic-like microstructure of  $\text{Ti}_4\text{Pt}_3 + \text{Ti}_3\text{Pt}$  (dark).

Figure 3. SEM image in backscattered mode of 42.7 at.% Pt, arc-melted. Remnants of  $\alpha$ -TiPt (white) within cored  $\text{Ti}_4\text{Pt}_3$  dendrites (medium greys), and intergranular eutectic-like microstructure of oxide +  $\text{Ti}_4\text{Pt}_3$ .

Figure 4. SEM image in backscattered mode of 42.7 at.% Pt, heat treated at 800°C 1 hour, and furnace cooled. Remnants of  $\alpha$ -TiPt (white) within cored  $\text{Ti}_4\text{Pt}_3$  dendrites (medium greys) and intergranular mixture of oxide +  $\text{Ti}_4\text{Pt}_3$  eutectic.

Figure 5. SEM image in backscattered mode of 46.7 at.% Pt, arc-melted. Laths of  $\alpha$ -TiPt (white) with  $\text{Ti}_4\text{Pt}_3$  (medium grey) at the former dendrite edges and intergranular eutectic-like microstructure of oxide +  $\text{Ti}_4\text{Pt}_3$  eutectic.

Figure 6. Comparison of X-ray spectra of sample containing  $\text{Ti}_4\text{Pt}_3$  with the JCPDS lines for  $\alpha$ -TiPt and  $\text{Ti}_3\text{Pt}$ .

Figure 7. SEM image in backscattered mode of 55.6 at.% Pt, arc-melted. Dendrites of  $\alpha$ -TiPt with laths and  $\alpha$ -TiPt (note laths) plus oxide eutectic.

Figure 8. Heating curves from differential thermal analysis of samples with between 31 and 44 at.% Pt, showing A, peak for  $\alpha$ -TiPt $\rightarrow\beta$ -TiPt displacive transformation; B, peak for presumed  $\text{Ti}_4\text{Pt}_3\rightarrow\text{Ti}_3\text{Pt}+\text{TiPt}$  reverse peritectoid transformation; C, peak for melting of eutectic; and D peaks associated with melting of primary  $\text{Ti}_3\text{Pt}$  or primary TiPt.

Figure 9. Cooling curves from differential thermal analysis of samples with between 31 and 44 at.% Pt, showing A, peak associated with solidification of  $\text{Ti}_3\text{Pt}$  and/or eutectic, B peak for peritectoid reaction  $\text{Ti}_3\text{Pt}+\text{TiPt}\rightarrow\text{Ti}_4\text{Pt}_3$ ; and C, peak for  $\beta$ -TiPt $\rightarrow\alpha$ -TiPt transformation.

Figure 10. Enthalpies of the reaction at 1215°C for  $\text{Ti}_4\text{Pt}_3\rightarrow\text{Ti}_3\text{Pt}+\text{TiPt}$ , plotted against platinum content. The approximate positions of the  $\text{Ti}_3\text{Pt}$ ,  $\text{Ti}_4\text{Pt}_3$ , TiPt and eutectic components have been overlaid.

Figure 11. Revised Ti-Pt phase diagram, showing new phase  $\text{Ti}_4\text{Pt}_3$ , increased melting point of  $\text{Ti}_3\text{Pt}$  and slightly modified  $\alpha/\beta$  boundary in TiPt.

*Revised and returned*

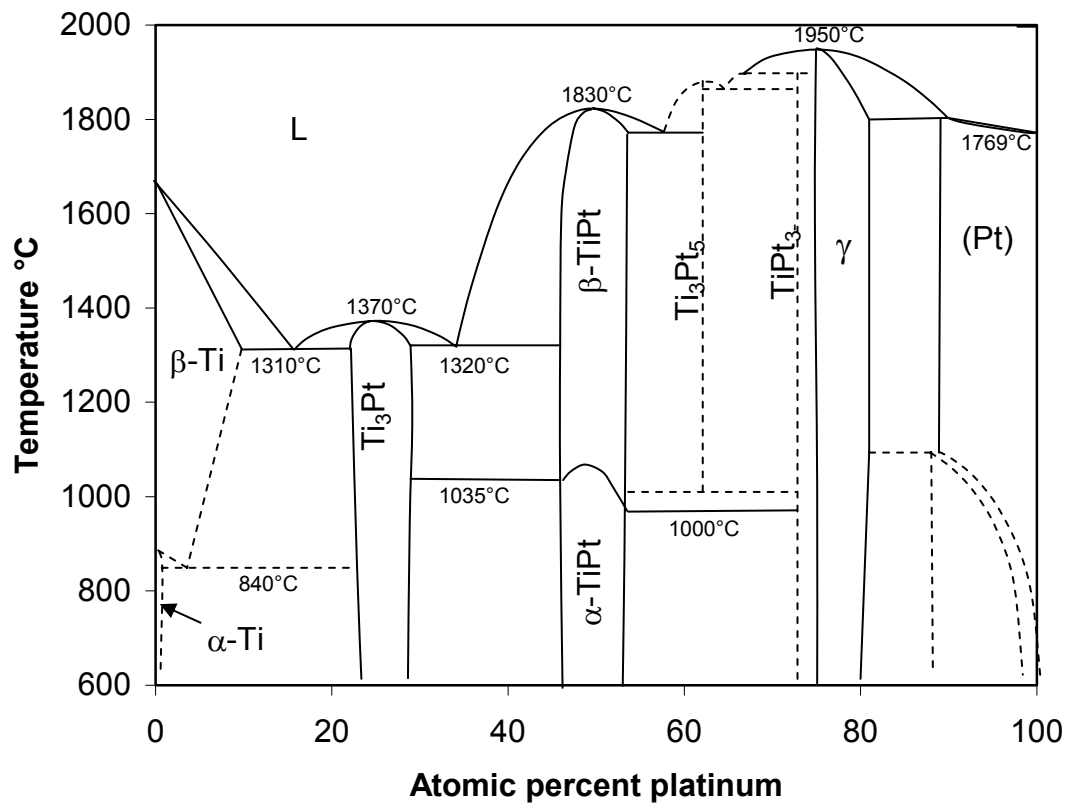


Figure 1. Ti-Pt phase diagram after Murray [1].

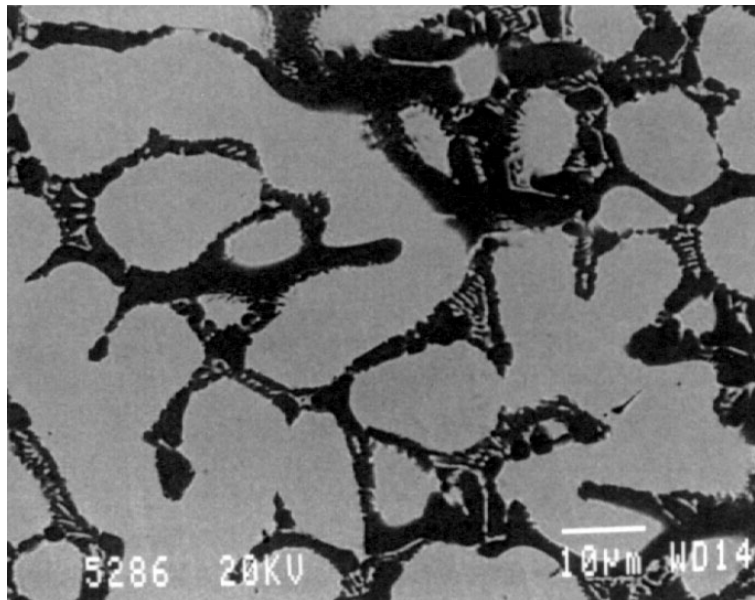


Figure 2. SEM image in backscattered mode of 37.6 at.% Pt, arc-melted, showing peritectoid conversion and growth of prior TiPt dendrites to  $\text{Ti}_4\text{Pt}_3$  (grey), with sparse eutectic-like microstructure of  $\text{Ti}_4\text{Pt}_3 + \text{Ti}_3\text{Pt}$  (dark).

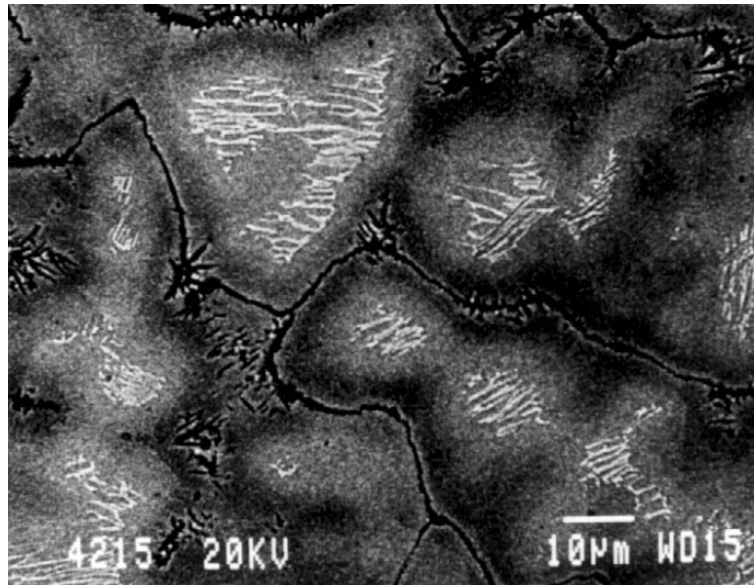


Figure 3. SEM image in backscattered mode of 42.7 at.% Pt, arc-melted. Remnants of  $\alpha$ -TiPt (white) within cored  $\text{Ti}_4\text{Pt}_3$  dendrites (medium greys), and intergranular eutectic-like microstructure of oxide +  $\text{Ti}_4\text{Pt}_3$ .

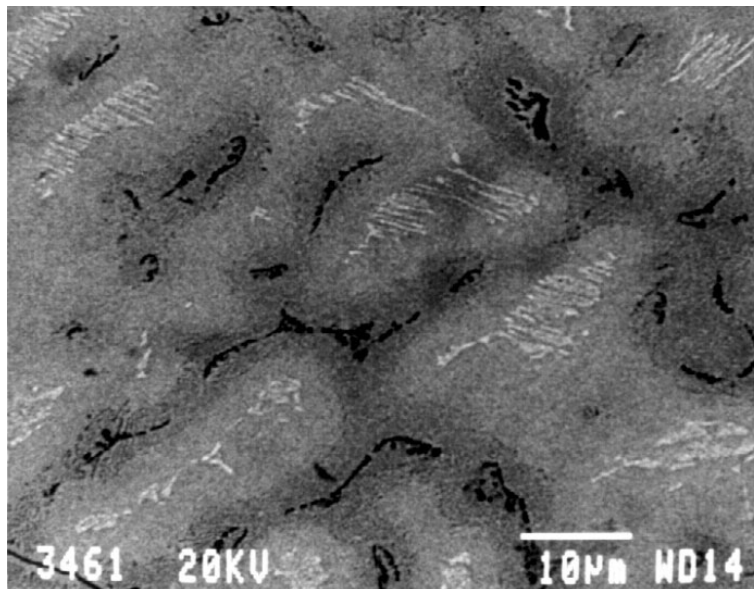


Figure 4. SEM image in backscattered mode of 42.7 at.% Pt, heat treated at 800°C 1 hour, and furnace cooled. Remnants of  $\alpha$ -TiPt (white) within cored  $\text{Ti}_4\text{Pt}_3$  dendrites (medium greys) and intergranular mixture of oxide +  $\text{Ti}_4\text{Pt}_3$  eutectic.

*Revised and returned*

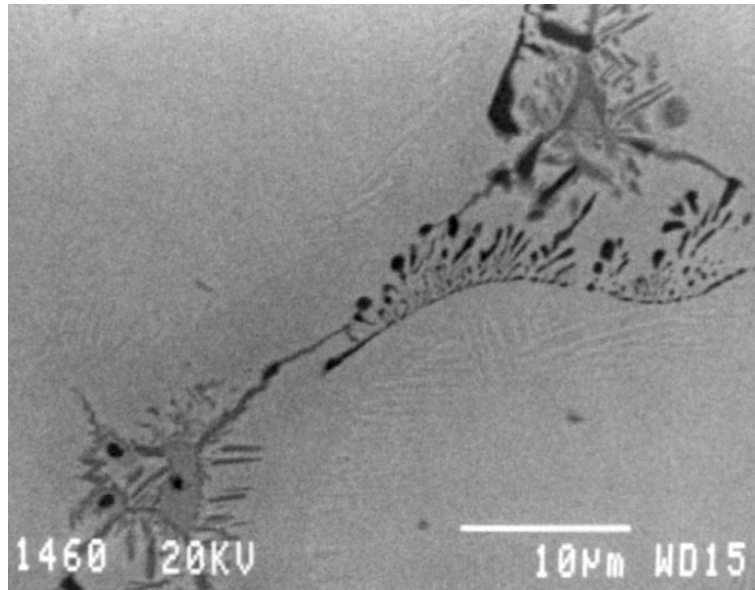


Figure 5. SEM image in backscattered mode of 46.7 at.% Pt, arc-melted. Laths of  $\alpha$ -TiPt (white) with  $\text{Ti}_4\text{Pt}_3$  (medium grey) at the former dendrite edges and intergranular eutectic-like microstructure of oxide +  $\text{Ti}_4\text{Pt}_3$  eutectic.

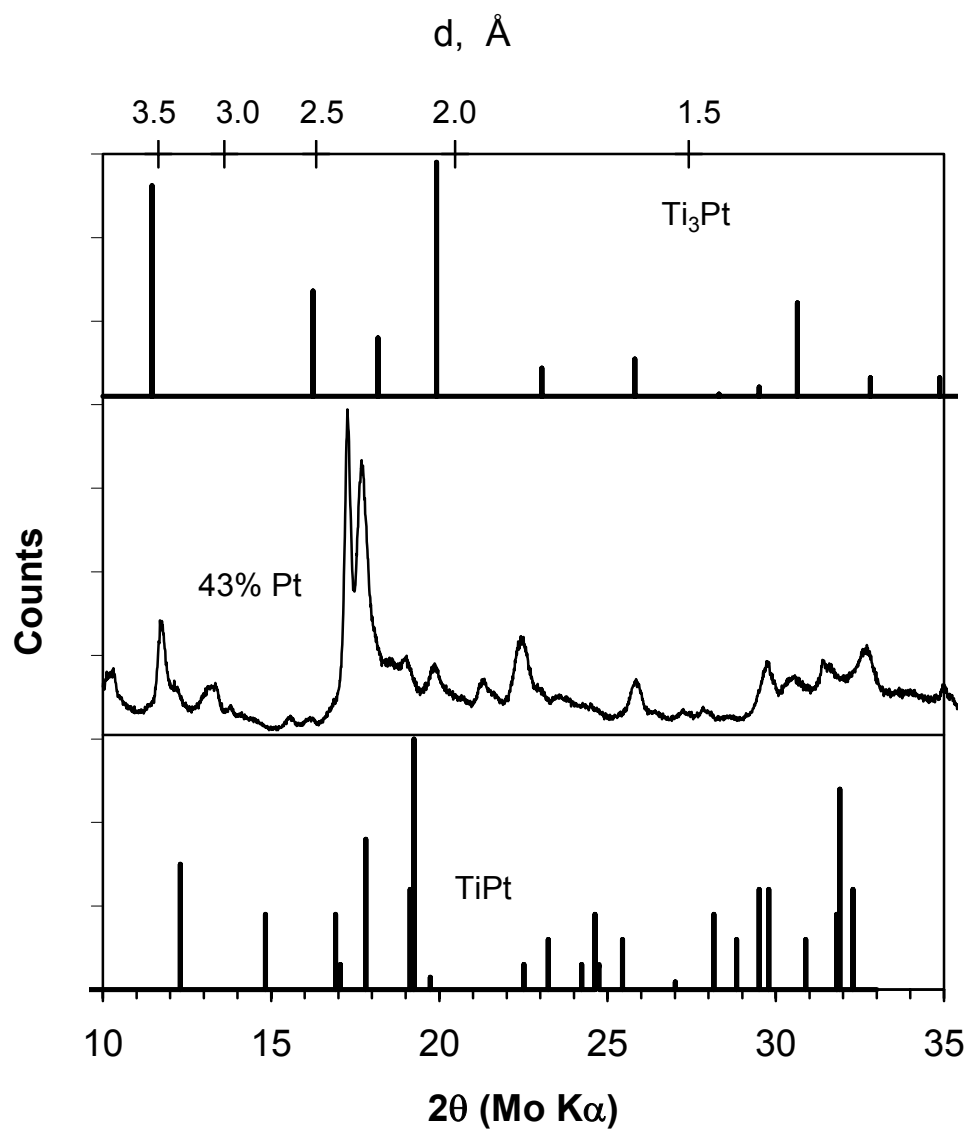


Figure 6. Comparison of X-ray spectra of sample containing  $Ti_4Pt_3$  with the JCPDS lines for  $\alpha-TiPt$  and  $Ti_3Pt$ .

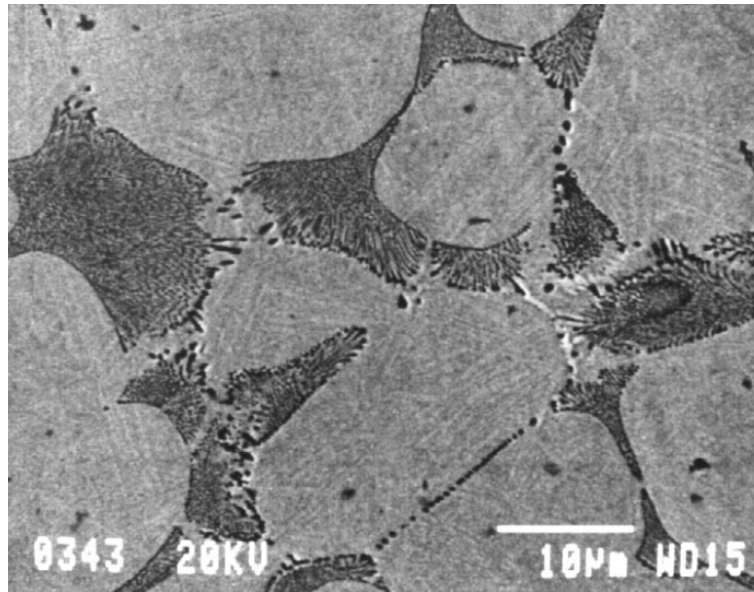


Figure 7. SEM image in backscattered mode of 55.6 at.% Pt, arc-melted. Dendrites of  $\alpha$ -TiPt with laths and  $\alpha$ -TiPt (note laths) plus oxide eutectic.

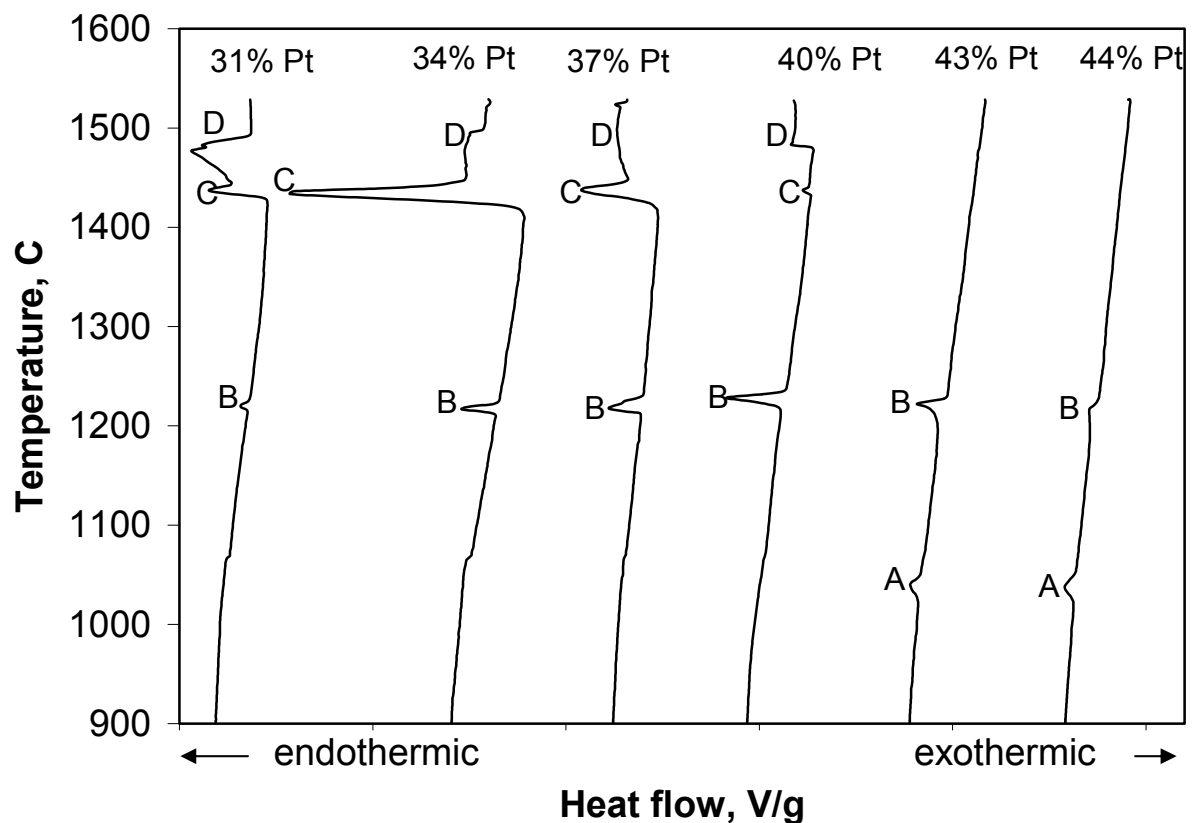


Figure 8. Heating curves from differential thermal analysis of samples with between 31 and 44 at.% Pt, showing A, peak for  $\alpha$ -TiPt  $\rightarrow$   $\beta$ -TiPt displacive transformation; B, peak for presumed  $\text{Ti}_4\text{Pt}_3 \rightarrow \text{Ti}_3\text{Pt} + \text{TiPt}$  reverse peritectoid transformation; C, peak for melting of eutectic; and D peaks associated with melting of primary  $\text{Ti}_3\text{Pt}$  or primary TiPt.

*Revised and returned*

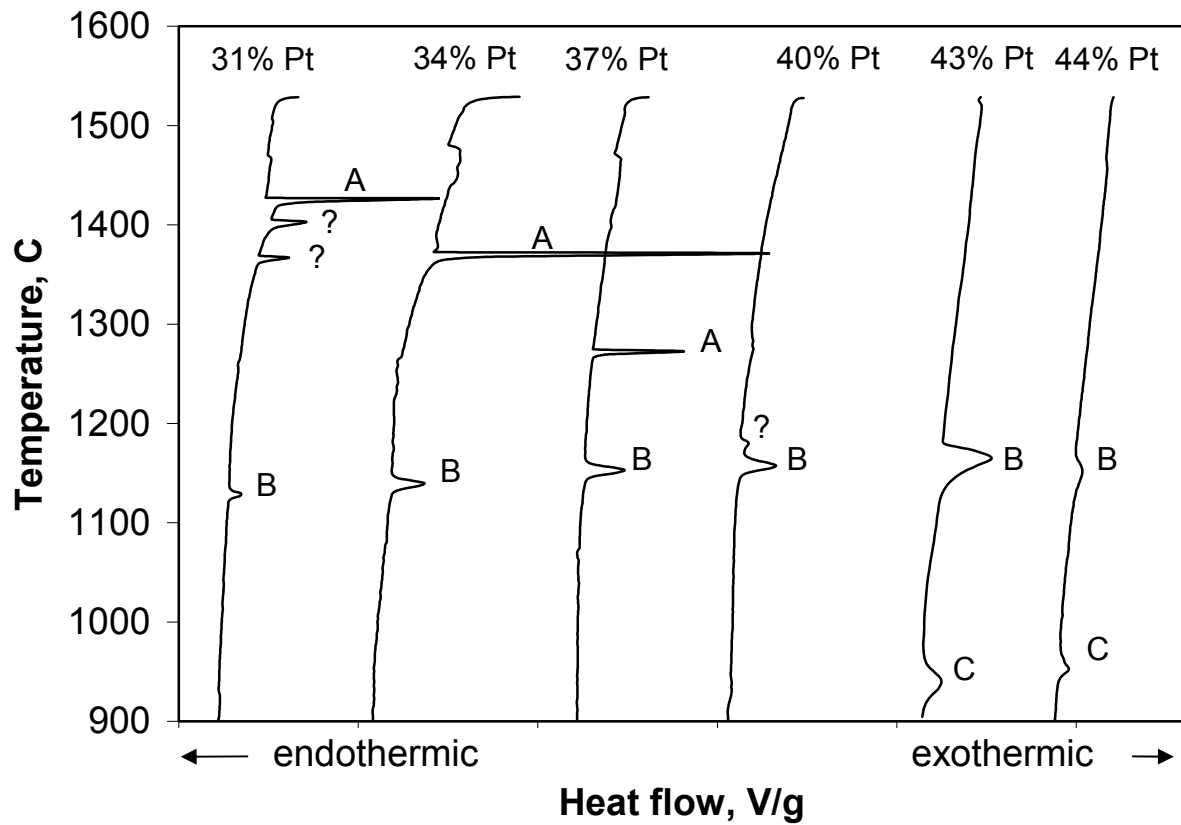


Figure 9. Cooling curves from differential thermal analysis of samples with between 31 and 44 at.% Pt, showing A, peak associated with solidification of  $\text{Ti}_3\text{Pt}$  and/or eutectic, B peak for peritectoid reaction  $\text{Ti}_3\text{Pt} + \text{TiPt} \rightarrow \text{Ti}_4\text{Pt}_3$ ; and C, peak for  $\beta\text{-TiPt} \rightarrow \alpha\text{-TiPt}$  transformation.

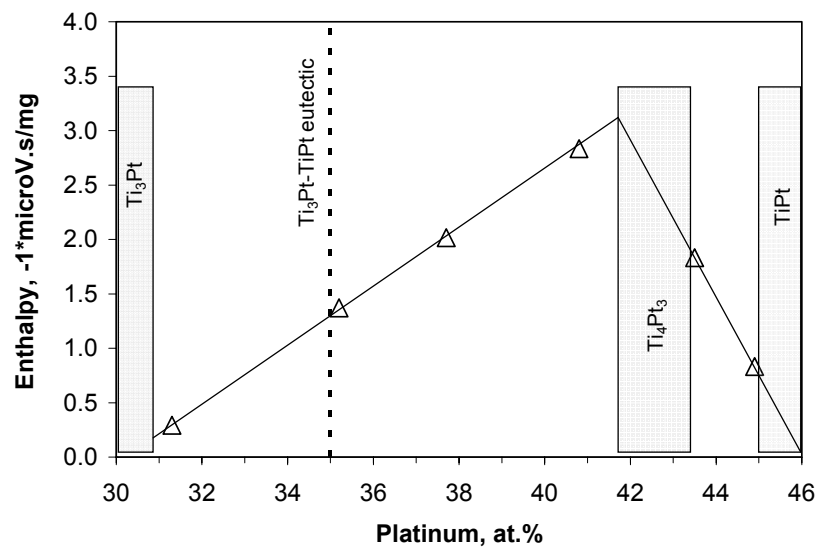


Figure 10. Enthalpies of the reaction at  $1215^\circ\text{C}$  for  $\text{Ti}_4\text{Pt}_3 \rightarrow \text{Ti}_3\text{Pt} + \text{TiPt}$ , plotted against platinum

*Revised and returned*

content. The approximate positions of the  $\text{Ti}_3\text{Pt}$ ,  $\text{Ti}_4\text{Pt}_3$ ,  $\text{TiPt}$  and eutectic components have been overlaid.

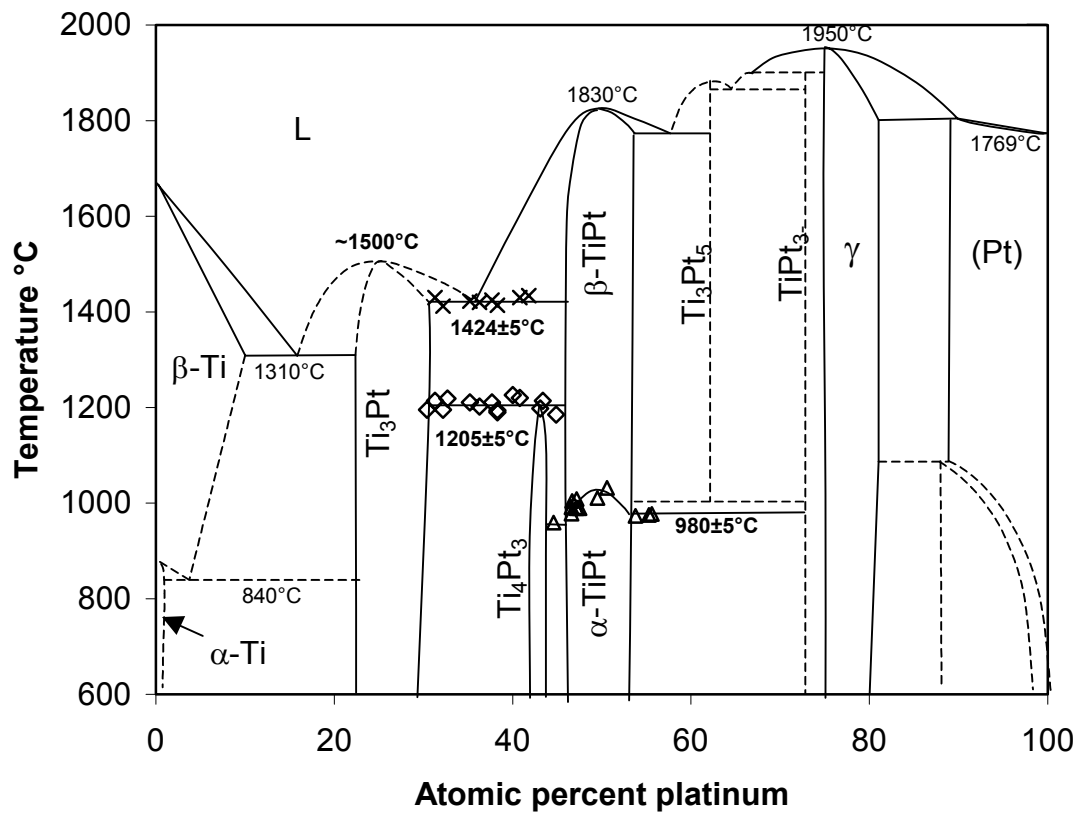


Figure 11. Revised Ti-Pt phase diagram, showing new phase  $\text{Ti}_4\text{Pt}_3$ , increased melting point of  $\text{Ti}_3\text{Pt}$  and slightly modified  $\alpha/\beta$  boundary in TiPt.



Overall	Ti <sub>3</sub> Pt	Eutectic overall	Ti <sub>4</sub> Pt <sub>3</sub>	αTiPt	Ti <sub>2</sub> Pt(O)	Ti <sub>3</sub> Pt <sub>5</sub>
30.2±0.5 H1	28.1±0.4	n/m	42.6±0.3	-	-	-
30.4±0.8	28.7±0.7	n/m	43.4±0.6	-	-	-
35.7±0.2 H1	29.3±1.9 e	34.1±2.1	41.3±2.2	-	-	-
36.3±0.8	30.7±0.5 e	34.8±0.9	42.4±0.5	-	-	-
37.6±0.5	30.4±0.4	n/m	41.7±0.5	-	-	-
40.7±0.5 H3	-	-	43.2±0.4	50.0±0.4	-	-
40.9±0.8	31.2±0.4	n/m	43.3±1.9	-	-	-
41.6±1.0	32.0±0.9	35.0±0.7	44.0±1.7*	-	-	-
42.0±0.9 H4	-	-	42.8±0.2	-	30.5±0.1	-
42.2±1.4 H3	-	-	43.3±0.4	50.3±0.5	-	-
42.3±0.2 H5	-	-	43.5±2.1	44.9±0.3 x	-	-
42.4±0.4 H1	-	-	42.8±0.4	45.5±0.1 x	32.0±0.5	-
42.7±0.9	-	-	42.6±0.5	45.1±0.9 x	-	-
43.1±0.5	-	-	42.2±0.5	45.0±0.5 x	-	-
43.1±0.5 H2	-	-	43.0±0.2	49.5±0.3	-	-
43.4±0.4 H4	-	-	-	45.7±1.1	34.3±0.4	-
46.6±0.6	-	n/m	~43	47.1±0.8	-	-
47.5±2.1	-	39.4±5.4 o	n/m	48.0±1.4	-	-
48.1±0.7	-	41.5±1.1 o	n/m	48.6±0.6	-	-
55.6±0.6	-	53.7±0.8 o?	-	56.1±0.9	-	-
55.3±0.6	-	-	-	58.4±1.2	29.8±2.3	-
56.8±0.1 H6	-	-	-	55.3±0.6	-	63.2±0.6
60.3±0.3 H6	-	-	-	52.4±0.5	-	62.5±0.3
61.3±0.6	-	-	-	56.0±1.0	-	63.7±0.3

Table 1. EDS Analyses of the alloys and phases examined. As-cast, unless otherwise specified.

Notes: n/m not measured; - not present; H1 800°C 1h fc; H2 1200°C 2h fc; H3 1200°C 60h fc; H4 1350°C 96h wq; H5 800°C 72h fc; H6 1200°C 72h wq; e measured within the eutectic; \* higher because Tipt present?; x has some Ti<sub>4</sub>Pt<sub>3</sub>; o eutectic with oxygen-containing phases?

*Revised and returned*

Table 2. XRD peaks ascribed to the  $\text{Ti}_4\text{Pt}_3$  phase from a sample with 43.1 at.% Pt (Mo radiation)

Lattice d-spacing (nm)	Intensity of peak, (as % of strongest peak on spectrum)
0.39642	7
0.34722	29
0.33566	9
0.30640	11
0.29597	5
0.24292	5
0.23649	100
0.23095	82
0.21529	18
0.20602	15
0.19229	10
0.18948	5
0.18263	23
0.17828	7
0.17414	5
0.17191	4
0.15883	13
0.13925	11
0.13829	18
0.13517	11
0.13099	18
0.12628	20
0.12130	6
0.11796	9
0.11070	4
0.09866	4
0.09115	4